INTERNATIONAL JOURNAL OF ONCOLOGY 68: 52, 2026

FOXM1 inhibitor, RCM-1, enhances venetoclax mediated apoptosis through downregulation of ATP2B4 in rhabdomyosarcoma

NAWAL MERJANEH[1-3*], YING-WEI LAN[3*], ZICHENG DENG[3], JOHNNY DONOVAN[4], GUOLUN WANG[4], JONATHAN DO[3], TIFFANY JUAN[3], XIAOMEI XIA[3], VLADIMIR V. KALINICHENKO[3,5] and TANYA V. KALIN[1-3]

[1]Center for Cancer and Blood Disorders, Phoenix Children's Hospital, Phoenix, AZ 85016, USA; [2]Department of Child Health, Division of Hematology and Oncology, The University of Arizona College of Medicine-Phoenix, Phoenix, AZ 85004, USA; [3]Phoenix Children's Research Institute, The University of Arizona College of Medicine-Phoenix, Phoenix, AZ 85004, USA; [4]Division of Neonatology and Pulmonary Biology, Perinatal Institute, Cincinnati Children's Research Foundation, Cincinnati, OH 45229, USA; [5]Division of Neonatology, Phoenix Children's Hospital, Phoenix, AZ 85016, USA

Received August 14, 2025; Accepted December 9, 2025

DOI: 10.3892/ijo.2026.5865

Abstract. Rhabdomyosarcoma (RMS) is the most common type of soft tissue sarcoma in children. Intensifying chemotherapy has failed to improve patient survival for metastatic or relapsed RMS and RMS survivors often suffer from significant long-term toxicities. More efficient and less toxic new therapies are critically needed. RMS expresses high levels of anti-apoptotic protein Bcl-2 and an oncogenic transcription factor Forkhead box protein M1 (FOXM1), which is also known to inhibit tumor cell apoptosis. The present study used a combination therapy of a recently developed non-toxic FOXM1 inhibitor, RCM-1 and the FDA-approved Bcl2 inhibitor, venetoclax, which is not effective as a monotherapy in solid tumors. Compared with venetoclax alone, the combination therapy efficiently inhibited RMS growth in the animal model by decreasing tumor cell proliferation and inducing tumor cell apoptosis. RNA-sequencing analysis demonstrated that the combination therapy uniquely decreased expression of ATPase Plasma Membrane Ca^{2+} Transporting 4 (ATP2B4), a plasma membrane calcium channel that is highly expressed in RMS compared with normal muscle cells. RCM-1, but not venetoclax treatment, inhibited ATP2B4 and enhanced the sensitivity of RMS cells to apoptosis. Knockdown of *ATP2B4* decreased RMS tumor cell proliferation, migration and colony formation *in vitro*. Furthermore, knockdown of *ATP2B4* increased tumor cell apoptosis, while overexpression of *ATP2B4* decreased tumor cell apoptosis *in vitro*. In the animal model of RMS, depletion of *ATP2B4* decreased tumor growth. In summary, combining RCM-1 with venetoclax sensitized RMS cells to apoptosis by decreasing ATP2B4. This made ATP2B4 a promising therapeutic target for RMS and provides a rationale for exploring this combination in early-stage clinical trials.

Correspondence to: Dr Nawal Merjaneh, Center for Cancer and Blood Disorders, Phoenix Children's Hospital, 1919 E Thomas Road, Phoenix, AZ 85016, USA
E-mail: nmerjaneh@phoenixchildrens.com

*Contributed equally

Key words: rhabdomyosarcoma, Forkhead box protein M1, ATPase Plasma Membrane Ca^{2+} Transporting 4, calcium signaling pathway, apoptosis

Introduction

Rhabdomyosarcoma (RMS) is the most prevalent soft tissue sarcoma in children and adolescents (1,2). Chemotherapy intensification has not improved the survival outcomes for metastatic or relapsed RMS (3,4). Moreover, the long-term side effects of chemotherapy are significant, including infertility and secondary malignancy. The heterogeneous genomic landscape of different types of RMS has challenged the introduction of targeted molecular therapies. Therefore, the search for molecular targets in RMS could allow for superior antitumor effects and fewer off-targeted side effects.

Forkhead box protein M1 (FOXM1) is a member of the forkhead box (FOX) transcription factor family that shares homology in the Forkhead DNA-binding domain (5,6). FOXM1 is a known oncogene that is highly expressed in various cancers with little to no expression in terminally differentiated cells (7-12). FOXM1 overexpression has been associated with advanced tumor stage and worse overall survival in many solid tumors, including rhabdomyosarcoma (13,14). Moreover, FOXM1 is notably upregulated in chemotherapy-resistant solid tumors, partly due to the role of FOXM1 in enhancing DNA repair response and protecting tumor cells from apoptosis (15,16). Collectively, FOXM1 contributes to multiple hallmarks of cancer (6,17).

Considering the essential role of FOXM1 in tumorigenesis, extended efforts have been directed towards identifying FOXM1 inhibitors (16). Using high throughput screening, a non-toxic, small molecule named Robert Costa Memorial Drug-1 or RCM-1 was developed (18). The anti-tumor efficacy and safety of RCM-1 were demonstrated in mouse models of different cancers. RCM-1 inhibited FOXM1 nuclear localization (18,19) and suppressed RMS tumor cell proliferation, colony formation and migration (19,20).

The B-cell lymphoma 2 (Bcl2) protein family regulates the intrinsic apoptotic pathway, balancing the pro- and anti-apoptotic proteins to maintain cellular homeostasis. Disturbing this balance to evade apoptosis is a hallmark of cancer (21). The anti-apoptotic protein Bcl2 is commonly expressed in rhabdomyosarcoma and has been associated with poor survival outcomes (22,23). Venetoclax, an FDA-approved Bcl2-specific inhibitor, is effective in hematologic malignancies but shows limited activity in solid tumors, necessitating rational combination therapies to enhance anti-tumor activity (24).

Previous preclinical RMS studies have shown that inhibiting Bcl2 has synergistic effects with chemotherapy (25-27). However, combining venetoclax with cytotoxic chemotherapy increases toxicity, notably prolonged neutropenia and thrombocytopenia (28). Therefore, the combination of venetoclax with targeted therapies such as RCM-1 may offer a more favorable safety profile.

The object of the present study was to determine whether the combination of RCM-1 and venetocalx exerted synergistic anti-tumor effects in RMS, while potentially offering fewer toxic side effects via targeting the apoptotic pathway.

Materials and methods

To evaluate the anti-tumor effects of RCM-1 and venetocalx in RMS, the present study performed a series of *in vitro* and *in vivo* experiments using mouse and human RMS cell lines. Cell viability, cytotoxicity and apoptosis were measured using CCK-8 and caspase 3/7 assay. To investigate the mechanism of synergy between RCM-1 and venetocalx, the present study performed RNA sequencing, followed by gene knockdown and overexpression, which were utilized for a series of *in vitro* and *in vivo* experiments, including immunofluorescence, reverse transcription-quantitative (RT-q) PCR and growth and migration assays.

Cell lines and reagents. RD and RH30 (ATCC) are fusion-negative and fusion-positive human RMS cells, respectively (29). 76-9 is a murine-derived RMS cell line isolated from a methylcholanthrene-induced mouse RMS tumor in a female C57BL/6 mouse and was provided by Dr Tim Cripe (Nationwide Children's Hospital, Columbus, OH, USA) (30,31). Human RMS cells were authenticated using STR profiling (Arizona Genetic Core). Cells were cultured in DMEM (76-9 and RD) or RPMI (RH30) complete media (Gibco; Thermo Fisher Scientific, Inc.) and kept at 37˚C and a 5% CO_2 incubator. The small molecule compound RCM1 (2-[2-oxo-2-(thiophen-2-yl) ethyl]sulfanyl-4,6-di(thiophen-2-yl) pyridine-3-carbonitrile) was synthesized by Vitas-M Laboratory (95% purity) and dissolved in DMSO for *in vitro* studies. Venetoclax (ABT-199) purchased from APeXBIO Technology LLC (cat. no. A8194) was dissolved in DMSO for *in vitro* studies and reconstituted in the solution that contained 10% ethanol, 30% polyethylene glycol 400 (PEG 400) and 60% lecithin dissolved in propylene glycol for *in vivo* studies.

Cell proliferation assays. 76-9 ($10x10^4$) and RD cells ($8x10^4$) per well were seeded in 6-well plates and allowed to grow for 24 h. RCM-1 was added at 24 h and venetoclax was added at 48 h in the sequential treatment regimen. Trypan blue staining was performed by incubating the cell suspension with 0.4% trypan blue at room temperature for 1 min. to exclude dead cells and viable cells were counted using a hemocytometer. To measure cell viability, cells were incubated with the cell counting kit-8 (CCK8) solution (GLPBIO Technology LLC) at 37˚C for 1 h, followed by detecting the absorbance at 450 nm using a microplate reader. Experiments were performed in triplicate.

Caspase 3/7 activation assay. Apoptosis in RMS cells following treatment with RCM-1 and venetoclax was assessed using the Caspase-Glo® 3/7 Assay (Promega Corporation) according to the manufacturer's protocol. After 72 h of drug incubation, as aforementioned, the Caspase-Glo 3/7 reagent was added to each sample at a 1:1 ratio with the culture volume. The plate was then incubated at 37˚C for 30 min and luminescence was subsequently measured using a microplate reader.

Nanoparticle synthesis. All chemicals for nanoparticle synthesis were used as received without any further purification and were obtained from MilliporeSigma.

The Poly(β-Amino Ester) (PBAE) polymer backbone was synthesized via a modified Michael Addition, as described in our previous studies (20,32). Briefly, Bisphenol A glycerolate diacrylate was initially mixed with 6-amino-1-hexanol in DMSO at 90˚C for 24 h. Following this, 4,4'-Trimethylenedipiperidine in DMSO was added to the mixture as the temperature was reduced to 50˚C and maintained for another 24 h. The PBAE backbone was then capped with methoxypolyethylene glycol amine and folic acid-modified polyethylenimine in DMSO at 40˚C. The folic acid modification was performed via EDC/NHS coupling, as previously described (33). To encapsulate RCM-1, the PBAE polymers were mixed with RCM-1 in DMSO at a mass ratio of 10:1, followed by transitioning the mixture to an aqueous environment to facilitate DMSO diffusion and nanoparticle self-assembly. The resulting nanoparticles were then dialyzed for 48 h to remove DMSO, excess drug and extra polymers. The concentration of RCM-1 encapsulated in the nanoparticles was determined by UV/Vis spectroscopy as described (34).

Mouse model. A total of 55 C57Bl/6J mice (8-12 weeks old, 1:1 male and female) were purchased from the Jackson Laboratory. The mean male mouse weight was 25 g and the average female mouse weight was 20 g. All mice were kept under SPF (specific-pathogen-free) conditions in 12-h light/dark cycle, 18-23˚C and 40-60% humidity. To generate the subcutaneous syngeneic murine model, $1x10^6$ 76-9 rhabdomyosarcoma cells were re-suspended in equal volumes of PBS: Matrigel (Corning, Inc.) and were injected subcutaneously into the flanks of mice (35). On day 7 after tumor cell inoculation, tumor-bearing mice were randomly assigned into control (n=19), single-agent RCM-1 (n=12), venetocalx (n=12), or combination therapy (n=12) groups. RCM-1 encapsulated into nanoparticles was prepared as previously described (RCM-1 NP^{FA}) (20) and administered via tail vein injection every other day for a total of seven injections, using the half-maximal inhibitory concentrations (IC_{50}) dose of 8 μg. Venetoclax (100 mg/kg/dose) was administered via oral gavage 5 days a week for 2 weeks. Control mice were injected and orally given a vehicle control. Tumors were harvested on day 21. Mice were monitored for signs of distress and weighed every other day until day 21. Mice were euthanized using IP pentobarbital (100 mg/kg/dose) followed by cervical dislocation to ensure irreversible death (36,37). Tumors were measured using calipers and volumes were calculated in cubic millimeters using $V=0.5xLxW^2$, where L was the tumor length and W was the tumor width.

Generating gene knockdown and overexpression in RMS cells. To knockdown *ATP2B4 in vitro*, RMS cells were transfected with SMARTpool siRNA (Horizon Discovery; cat. no. L-066791-00-0010) and non-targeting siRNA pool as a control (Horizon Discovery; cat. no. D-001810-10) by using Dharmafect transfection reagent (Dharmacon, Inc.; Revvity, Inc.) as previously described (38). For stable knockdown of ATPase Plasma Membrane Ca^{2+} Transporting 4 (*Atp2b4*) in 76-9 cells, pre-packaged lentiviral particles containing ATP2B4 short hairpin (sh)RNA were purchased directly from Origene (cat. no. TL508592V; titer $4.8x10^7$ TU/ml). Wild-type (WT) 76-9 cells were transduced with two mouse lentiviral particles (C, D) at a multiplicity of infection (MOI=50) in the presence of 8 μg/ml polybrene, and incubated at 37˚C overnight. Medium was replaced the following day, and cells were cultured for 48-72 h. GFP^+ transfected cells were isolated by FACS. Briefly, cells were dissociated into a single-cell suspension, washed with PBS, resuspended in culture medium and filtered through a 40-μm cell strainer prior to sorting. GFP^+ cells were gated based on unstained control cells and collected using a Sony SH800 cell sorter. FACS analysis was performed as previously prescribed (18). To knockdown *FOXM1,* 76-9 and RH-30 were transfected with pLKO-*shFOXM1* plasmid DNA (clone ID: TRCN0000015546; MilliporeSigma) against *FOXM1*using TransIT-X2 (Mirus Bio, LLC; cat. no. MIR 6004). To overexpress ATP2B4a and ATP2B4b, 76-9 cells were transfected with CMV-ATP2B4a (Origene; cat. no. MC223809) and CMV-ATP2B4b (Origene; cat. no. MR215322) or an empty overexpression (OE) plasmid as a control. For both FOXM1 knockdown and ATP2B4 overexpression transfections performed using TransIT-X2, cells were plated at $8x10^4$ cells per well in a 24-well plate and transfected with 0.5 μg plasmid DNA premixed with 1.5 μl TransIT-X2, followed by incubation at 37˚C for 24 h before subsequent selection or analysis. Sequences are listed in Table SI.

Immunofluorescence staining. Control, siATP2B4 and pATP2B4 76-9 cells were seeded at a density of $1x10^5$ cells per 24 mm square coverslip in 6-well plates and allowed to grow for 48 h. Cells were then fixed in 4% paraformaldehyde at room temperature for 15 min, washed three times with PBS, and stained as previously described (20). Blocking was performed using 4% Normal Goat Serum (Jackson ImmunoResearch Labs; cat. no. 005-000-121) at room temperature for 3 h. Primary antibodies were incubated overnight at 4˚C, followed by secondary antibody incubation at room temperature for 1 h, during which Hoechst 33342 (Invitrogen; Thermo Fisher Scientific, Inc.; cat. no. H3570) was included as a nuclear counterstain. For quantification, five random fields per sample were acquired at 20x magnification using the EVOS FL Auto 2 Cell Imaging System and EVOS imaging software (Thermo Fisher Scientific, Inc.). To perform immunostaining of tumor tissue, paraffin-embedded 76-9 subcutaneous tumor sections were stained as described previously (39). Briefly, tissues were fixed in 4% paraformaldehyde at 4˚C overnight, dehydrated through graded ethanol and xylene, and embedded in paraffin at 60˚C. Sections (5 μm) were deparaffinized, rehydrated, and subjected to antigen retrieval in citrate buffer (pH 6.0) at 95˚C for 20 min. Slides were blocked with 4% Normal Goat Serum at room temperature for 1 h, incubated with primary antibodies overnight at 4˚C, and then incubated with secondary antibodies at room temperature for 1 h with Hoechst 33342 included as a nuclear counterstain. Five random fields per sample were acquired and quantified using ImageJ, with imaging performed on the same EVOS FL Auto 2 platform. Antibodies used for immunostaining were anti-Ki-67 (1:250; Invitrogen, MA5-14520), anti-Cleaved-Caspase 3 (1:200; R&D, MAB835), anti-BAX (1:150; Santa Cruz, sc-7480), anti-ATP2B4 (1:200; Thermo Fisher Scientific, Inc.; cat. no. PA5-87634).

RT-qPCR. RNA was isolated using the RNeasy kit (Qiagen; cat. no.74104) and was subsequently reversed to cDNA using the iScript cDNA synthesis kit (Bio-Rad Laboratories, Inc.; cat. no.1708891). qPCR was carried out using TaqMan Gene Expression Assays (Applied Biosystems) according to the manufacturer's instructions. The thermal cycling conditions were: An initial hold at 50˚C for 2 min, followed by 95˚C for 10 min, and 45 cycles of 95˚C for 15 sec and 60˚C for 1 min (annealing/extension with data acquisition). Experiments were performed in triplicates, and relative gene expression was analyzed using the $2^{-\Delta\Delta Cq}$ method (40). Assay catalog numbers are provided in Table SII.

Clonogenic growth assay. Control and small interfering (si)ATP2B4 knockdown 76-9 cells were seeded at 2,000 cells per well in 6-well culture plates and cultured in a 37˚C, 5% CO_2 incubator. The culture medium was replaced every 2 days. After 6 and 9 days in culture, the cells were washed with Dulbecco's phosphate-buffered saline (DPBS), fixed with 4% paraformaldehyde (PFA) for 10 min at room temperature and then treated with 100% ice-cold methanol for 5 min to permeabilize the cells. Subsequently, the cells were stained with 0.5% crystal violet (dissolved in 25% methanol) for 10 min at room temperature. After staining, the crystal violet solution was removed and the cells were washed with DPBS at least twice to achieve a clear background. Representative images were captured and the crystal violet staining was quantified using ImageJ software (version 1.53e; National Institutes of Health).

Wound healing assay. Ibidi two-well culture inserts (Ibidi GmbH; cat. no.80209) were used for the experiment. A total of 4×10^4 control or siATP2B4 knockdown 76-9 cells were seeded into the culture inserts and allowed to adhere overnight. Cells were maintained in complete growth medium. Afterward, the culture inserts were removed, creating open areas with clear edges. Images of these open areas were captured using the EVOS FL Auto 2 Cell Imaging System (Thermo Fisher Scientific, Inc.) at 0, 6 and 24 h using a light (phase-contrast) microscope, the EVOS FL Auto 2 Cell Imaging System (Thermo Fisher Scientific, Inc.). The images were analyzed using TScratch software (CSElab; ETH Zurich; version 1.0).

Fura-2 AM staining. 76-9 cells were transfected with siAtp2b4 or a non-targeting control (siNC) for 24 h, then stained with 5 μM Fura-2 AM (AAT Bioquest; cat. no. 21020) in a 37˚C, 5% CO_2 incubator. After 30 min of incubation, the cells were rinsed with DPBS and images were captured using the EVOS FL Auto 2 Cell Imaging System (Thermo Fisher Scientific, Inc.).

Apoptosis measurement and Caspase 3 activation assay. Control, siATP2B4 and ATP2B4 overexpressed 76-9 cells were seeded in a 24-well plate at a density of 8×10^4 cells/ml overnight and treated with venetoclax (5 and 8 μM) for 24 h. Then, apoptotic cells were assessed via Annexin V-iFluor 488 staining and Caspase 3 activity was measured using TF3-DEVD-FMK staining with the Cell Meter Live Cell Caspase 3/7 and Phosphatidylserine Detection Kit (AAT Bioquest; cat. no. 22850). Cells were incubated with Annexin V–iFluor 488 and TF3-DEVD-FMK at 37˚C in a 5% CO_2 incubator for 1 h, followed by Hoechst staining at room temperature for 10 min. Fluorescence images were captured and analyzed using the EVOS FL Auto 2 Cell Imaging System (Thermo Fisher Scientific, Inc.). The apoptotic rate was calculated as the percentage of Annexin V-positive cells, including both early and late apoptotic populations, relative to the total number of Hoechst-positive cells.

RNA-sequencing (RNA-seq) and data analysis. RNA extracted from control and treated 76-9 cell line were sent to the CCHMC Genomics Sequencing Facility, Cincinnati, Ohio (USA) for sequencing. The quality of RNA was determined using a Fragment Analyzer with an average RNA Quality Number for all samples of 9.87. RNA libraries were prepared for all samples using Illumina Stranded total RNA Prep, Ligation with Ribo-Zero (Illumina, Inc.) to generate non-stranded RNA libraries. Sequencing was performed using NoveSeq6000 (Illumina, Inc.) with an estimated 30 million read per sample. Reads were aligned to the GRCm38 mouse genome and quantified using an index transcriptome version of GRCm38 using *Kallisto* and standard settings. This was performed by the CCHMC Genomics Sequencing Facility, Cincinnati, Ohio (USA). Raw counts were normalized using DESeq2 (41). Differential gene expression between conditions was performed using DEseq2, which uses a negative binomial model for each gene. The Wald test was used for hypothesis testing when comparing the two groups. All P-values attained were corrected for multiple testing using the Benjamini and Hochberg method, which is the default method in DESeq2. In the standard DESeq2 algorithm, the α for the false-discovery rate is set to 0.1 by default. Heatmap was generated using the *pheatmap* R package (version 1.0.12; https://cran.r-project.org/package=pheatmap) and the volcano plot was generated using the *EnhancedVolcano* R package (https://github.com/kevinblighe/EnhancedVolcano). Venn diagrams for differentially expressed genes were created using AltAnalyze (42). Gene list functional enrichment was created using TopGene Suite and graphed using sRplot (43,44).

Single-cell RNA-seq data analysis. The datasets GSE143704 (45) and GSE195709 (46) were obtained from the GEO database (https://www.ncbi.nlm.nih.gov/geo/query/acc.cgi?acc=GSE143704 and https://www.ncbi.nlm.nih.gov/geo/query/acc.cgi?acc=GSE195709). The GSE143704 dataset contains muscle tissue cell populations from 10 healthy human donors, while the GSE195709 dataset includes rhabdomyosarcoma samples from 4 primary rhabdomyosarcoma patients. The datasets were both generated using the NextSeq 500 platform (Illumina, Inc.). Data analysis was performed using the Seurat R package (version 4.3.1; https://satijalab.org/seurat/). Cells with >100 genes detected or with a mitochondrial gene percentage >20% were excluded. The present study used the FindClusters and FindAllMarkers functions in Seurat to identify clusters for Smooth Muscle Cells (ACTA2), Skeletal Muscle (ACTA1) and Myoblasts (PAX7). These three clusters were then integrated with the scRNA-seq dataset of the 4 rhabdomyosarcoma samples using the SCTintegration function of the Seurat package. The cells were clustered using the FindClusters function and cluster visualization was performed using Uniform Manifold Approximation and Projection (UMAP). ATP2B4 expression levels were analyzed to generate a violin plot.

Cloning of the human ATP2B4 promoter region and the luciferase reporter assay. The human *ATP2B4* promoter region spanning-373 to 0 bp was obtained from 293 genomic DNA through PCR amplification using the following primers (5'-3'): Forward: TGAGCAAGAGTCTGGCCCGGGGTACCCC; reverse: GGGGTACCCCGGGCCAGACTCTTGCTCA. This promoter region was then cloned into the *Kpn*I site of the pGL4.23[luc2/minP] luciferase reporter plasmid (Promega Corporation). A Dual-Glo luciferase reporter assay was performed on 76-9 cells, which were co-transfected with the luciferase reporter, *Renilla* and either a CMV-empty or CMV-FOXM1 overexpression plasmid.

Statistical analysis. Data were expressed as mean ± SD. Statistical significance was determined using an unpaired Student's t-test, or one-way or two-way analysis of variance (ANOVA) followed by Tukey's multiple comparisons post hoc test, where appropriate. The *in vivo* experiment was a pilot study with no formal power calculation required and was analyzed in a blinded manner. All statistical analyses were obtained using GraphPad Prism (version 9.5.1; Dotmatics). $P<0.05$ was considered to indicate a statistically significant difference.

Results

The sequential treatment of RCM-1 and venetoclax decreases RMS cell viability and enhances apoptosis in vitro. To establish the IC_{50} of RCM-1 and venetoclax, mouse 76-9 and human RD rhabdomyosarcoma cell lines were treated with increasing doses of RCM-1 and venetoclax to generate a dose-response curve. The IC_{50} of RCM-1 was 2.5 μM in RD cells and 1.37 μM in 76-9 cells, whereas venetoclax had higher IC_{50} values of 9.4 μM in RD cells and 6.3 μM in 76-9 cells (Fig. S1A). Next, RMS cells were treated with either RCM-1 alone, venetoclax alone, or a combination of both agents sequentially. The combination therapy of RCM-1 and venetocalx reduced the number of viable tumor cells by 70% compared with 40-50% with single agents (Fig. 1A and B). Also, the CCK8 assay showed a significant reduction in RD, 76-9 and RH30 cell viability after RCM-1 and venetocalx treatment compared with a single agent or vehicle (Figs. S1B and C). Next, caspase 3/7 activity was assessed using Caspase-Glo® 3/7 Assay kit. The combination therapy significantly increased apoptosis in RD, 76-9 and RH30 cells compared with single agents (Figs. 1C and S1C). Thus, the combination of RCM-1 and venetoclax inhibits RMS tumor cell growth and induces apoptosis more efficiently than either drug alone.

Combination therapy with RCM-1-NP^{FA} and venetoclax inhibits tumor growth and promotes tumor cell apoptosis in the mouse model of RMS. To verify that the efficacy of combination therapy is not limited to *in vitro* conditions, a mouse model of RMS was used. 76-9 RMS tumor cells were inoculated subcutaneously into the flanks of C57Bl/6J mice. The tumor-bearing mice were randomly assigned to 4 groups and were treated with either vehicle (control), venetoclax alone, IC_{50} dose of nanoparticle-encapsulated RCM-1 alone, or a combination of both drugs (20) (Fig. 2A). Monotherapy with venetoclax did not have anti-tumor efficacy in the RMS mouse model (Fig. 2B), which is consistent with previously published studies (26,47) (Fig. 2B). Monotherapy with the IC_{50} dose of RCM-1-NP^{FA} had only limited anti-tumor efficacy (Fig. 2B). However, the combination therapy efficiently reduced RMS tumor growth in a mouse model (Fig. 2B). The combination therapy effectively suppressed cell proliferation, as indicated by the decreased number of Ki-67 positive cells, and significantly promoted apoptosis, evidenced by the increased percentage of BAX and cleaved caspase-3 positive cells compared with single agents (Fig. 2C-E). The combination therapy was well tolerated in mice, with no observed weight loss throughout the experiment (Fig. S2A). Venetoclax-treated mice exhibited reduced white blood cell counts compared with controls (Fig. S2B), consistent with known myelosuppressive effects of venetoclax in humans. Importantly, the combination therapy did not induce liver dysfunction (Fig. SC). Thus, the combination of RCM-1-NP^{FA} and venetoclax efficiently inhibits tumor growth and is not toxic in the animal model of RMS.

RNA-seq analysis identifies a signature of cellular stress in the combination therapy. To determine the molecular mechanism of increased apoptosis in the combination therapy, bulk RNA sequencing was performed to compare the transcriptome of untreated control and treated 76-9 RMS cells (Fig. 3A). The gene enrichment analysis of RMS cells treated with the combination therapy compared with venetoclax revealed an upregulation in multiple biologic pathways that are activated in cells under stress, such as ferroptosis, unfolded protein response and oxidative stress response. The cytosolic Ca^{2+} level pathway was significantly elevated in the combination therapy compared with venetoclax as well. The downregulated pathways included WNT signaling, mitotic cell cycle, hypoxia-inducible factor-1α signaling, Hippo signaling, TGF-β signaling, AKT-mTOR and FOXM1 network pathways, reflecting the role of RCM-1 in FOXM1 inhibition (Fig. 3B). A volcano plot was generated to visualize the most differentially expressed genes in combination therapy compared with venetoclax treatment (Fig. 3C). *Atp2b4* was one of the most downregulated genes in the combination treatment. The decreased expression of *Atp2b4* mRNA was confirmed using RT-qPCR, demonstrating that both RCM-1 treatment and combination therapy were sufficient to decrease the *Atp2b4* mRNA level (Fig. 3D). Furthermore, using immunofluorescence staining, the present study showed that the protein level of ATP2B4 was also decreased in RMS tumors after RCM-1 or combination treatment (Fig. 3E).

ATP2B4 is differentially expressed in rhabdomyosarcoma cells and is essential for RMS cell proliferation and migration. Since it has been shown that ATP2B4, a calcium channel located on the plasma membrane, plays an important role in different cancers (48,49), the present study analyzed the publicly available sc-RNA genomic databases of human normal muscle tissue and RMS tumors (45,46) (Figs. S3A and 4A). Consistent with previously published data, *Bcl2* was overexpressed in RMS (22,23) and *CDKN1A* (a cell cycle inhibitor) was overexpressed in normal muscle cells (Fig. S3B). Based on the sc-RNA seq analysis, the mRNA level of *ATP2B4* was markedly higher in fusion-negative (RMS 1 and 3), fusion-positive (RMS 2) and spindle (RMS 4) rhabdomyosarcoma compared with normal human muscle cells, including skeletal muscle, smooth muscle cells and myoblasts (Fig. 4A). Also, ATP2B4 mRNA level was 3-4 fold higher in human RMS cell lines (RD and RH30) compared with normal skeletal muscle cells (HSkMC) (Fig. 4B). To determine the role of ATP2B4, 76-9 RMS cells were transfected with siRNA against *Atp2b4*, resulting in ~45% knockdown of *Atp2b4* mRNA after 24 h and ~87% after 48 h (Fig. S4A; left panel). Immunostaining also demonstrated that the protein level of ATP2B4 was decreased 24 h after siATP2B4 transfection (Fig. S4A; right panel). Depletion of ATP2B4 increased the basal cytosolic Ca^{2+} level in RMS tumor cells (Fig. 4C), which is consistent with the upregulated signaling pathway related to cytosolic Ca^{2+} levels shown in RNA seq pathway analysis (Fig. 3B). Furthermore, depletion of ATP2B4 in rhabdomyosarcoma cells led to a time-dependent decrease in tumor cell proliferation, with a 40% reduction observed at 72 h as well as reduced colony formation and cell migration (Fig. 4D-F). Thus, *ATP2B4* is differentially expressed in rhabdomyosarcoma cells and is essential for RMS cell proliferation and migration.

Knockdown of ATP2B4 enhances venetoclax-mediated apoptosis in 76-9 RMS cells. To determine whether ATP2B4 is important for venetoclax-induced apoptosis in

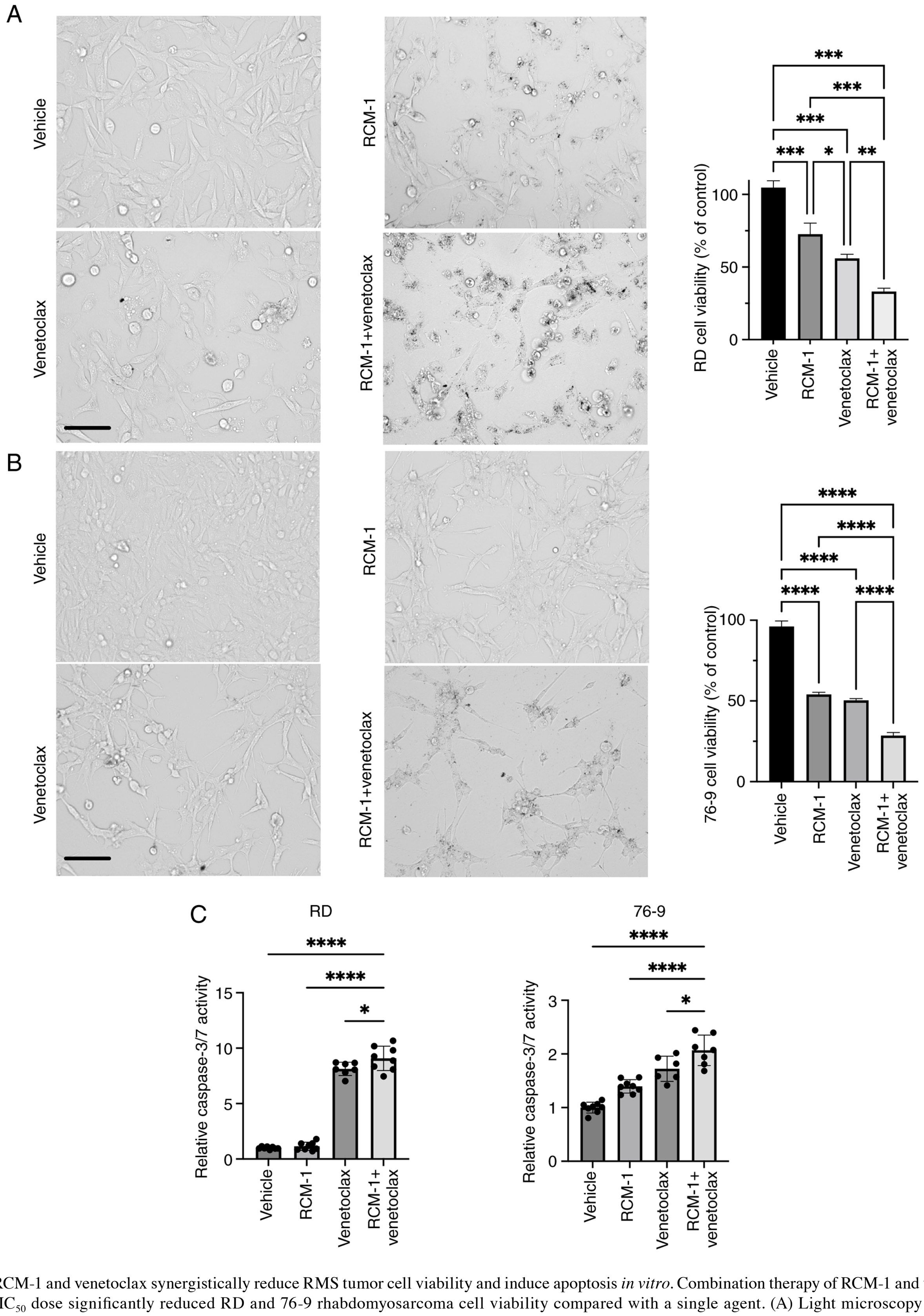

Figure 1. RCM-1 and venetoclax synergistically reduce RMS tumor cell viability and induce apoptosis *in vitro*. Combination therapy of RCM-1 and venetoclax using the IC_{50} dose significantly reduced RD and 76-9 rhabdomyosarcoma cell viability compared with a single agent. (A) Light microscopy images of RD cells treated with vehicle, single agent RCM-1, venetocalx, or combination therapy. (B) The same experiment was performed using 76-9 tumor cells. (C) Combination therapy significantly enhanced apoptosis in RD and 76-9 cells compared with either agent alone. Values are shown as mean ± SD. $^{*}P \leq 0.05$, $^{**}P \leq 0.01$, $^{***}P \leq 0.001$, $^{****}P \leq 0.0001$. Scale bar, 100 μm. RMS, rhabdomyosarcoma; IC_{50}, half-maximal inhibitory concentrations.

rhabdomyosarcoma, the present study treated control and ATP2B4-depleted tumor cells with increasing doses of venetoclax. Using immunostaining with antibodies against caspase 3/7 (DEVD) and annexin V, it was shown that venetoclax induced a dose-dependent increase in apoptosis of control tumor cells (Fig. 5A and B). Moreover, the depletion

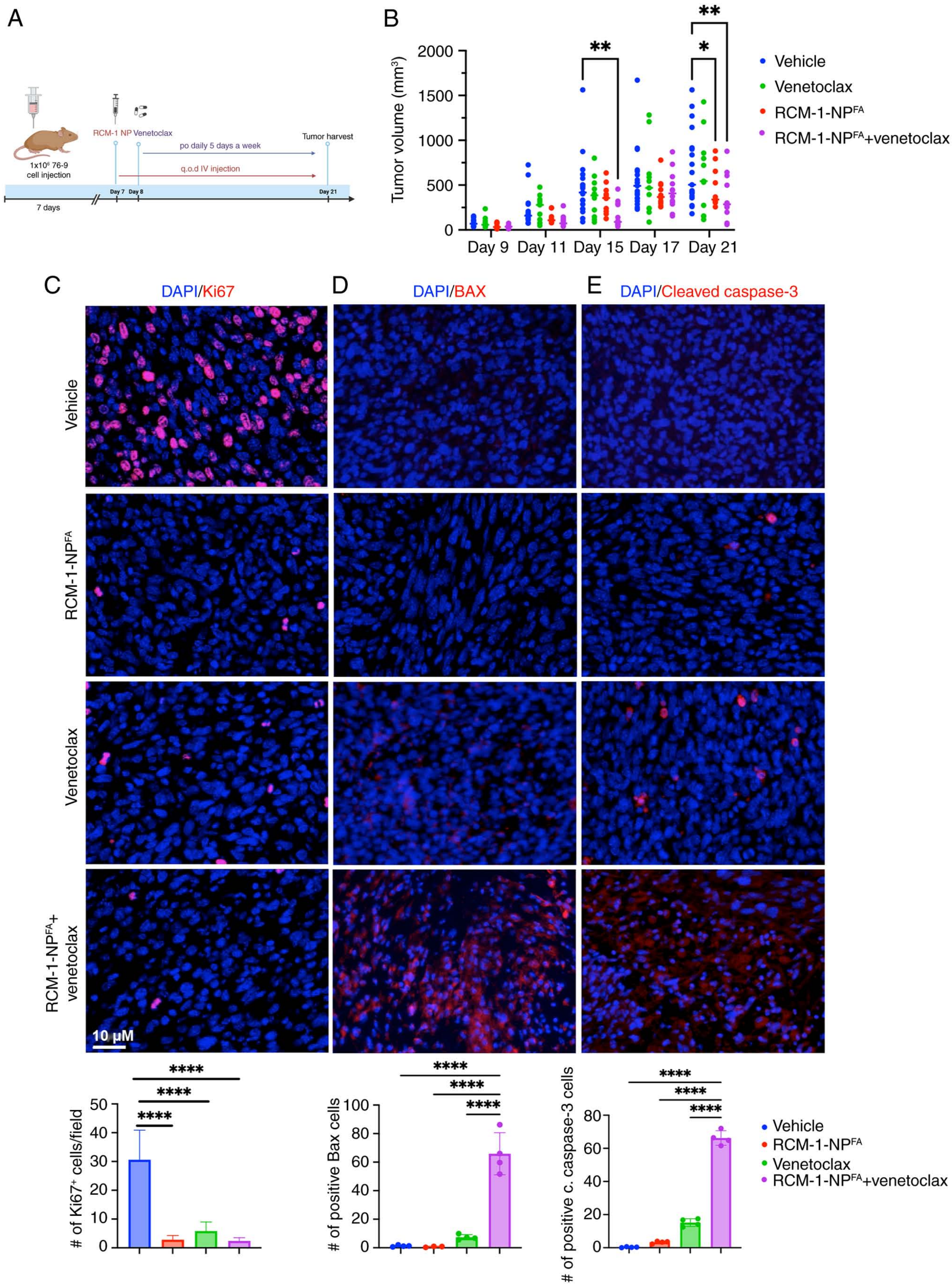

Figure 2. The combination of RCM1-NP^{FA} and venetoclax decreases tumor growth and enhances caspase-mediated apoptosis in a murine RMS model. (A) Schematic diagram of tumor cells inoculation and treatment. The figure is created in BioRender. Merjaneh, N. (2024) https://BioRender.com/z67t342. (B) Combination therapy significantly reduced tumor burden compared with vehicle. The mean vehicle tumor volume on day 21 was 685 mm^3, compared with the average tumor volume of the combination therapy of 361 mm^3. The maximum tumor diameter was 17.3x11.5 mm and the corresponding maximum tumor volume was 1,144 mm^3. Tumor volume was measured at different time points during the experiment (P≤0.01; n=12). (C) Combination therapy inhibited proliferation, as indicated by the decreased number of Ki67-positive cells. Combination therapy increased apoptosis, shown by the increased number of (D) BAX-positive cells and (E) the number of caspase3-positive cells compared with single agents and/or vehicle. A total of five random fields per sample were used to quantify the number of Ki67, BAX and cleaved caspase 3 positive cells per group. Values are shown as mean ± SD. Scale bar, 10 μm. *P≤0.05, **P≤0.01, ****P≤0.0001. RMS, rhabdomyosarcoma.

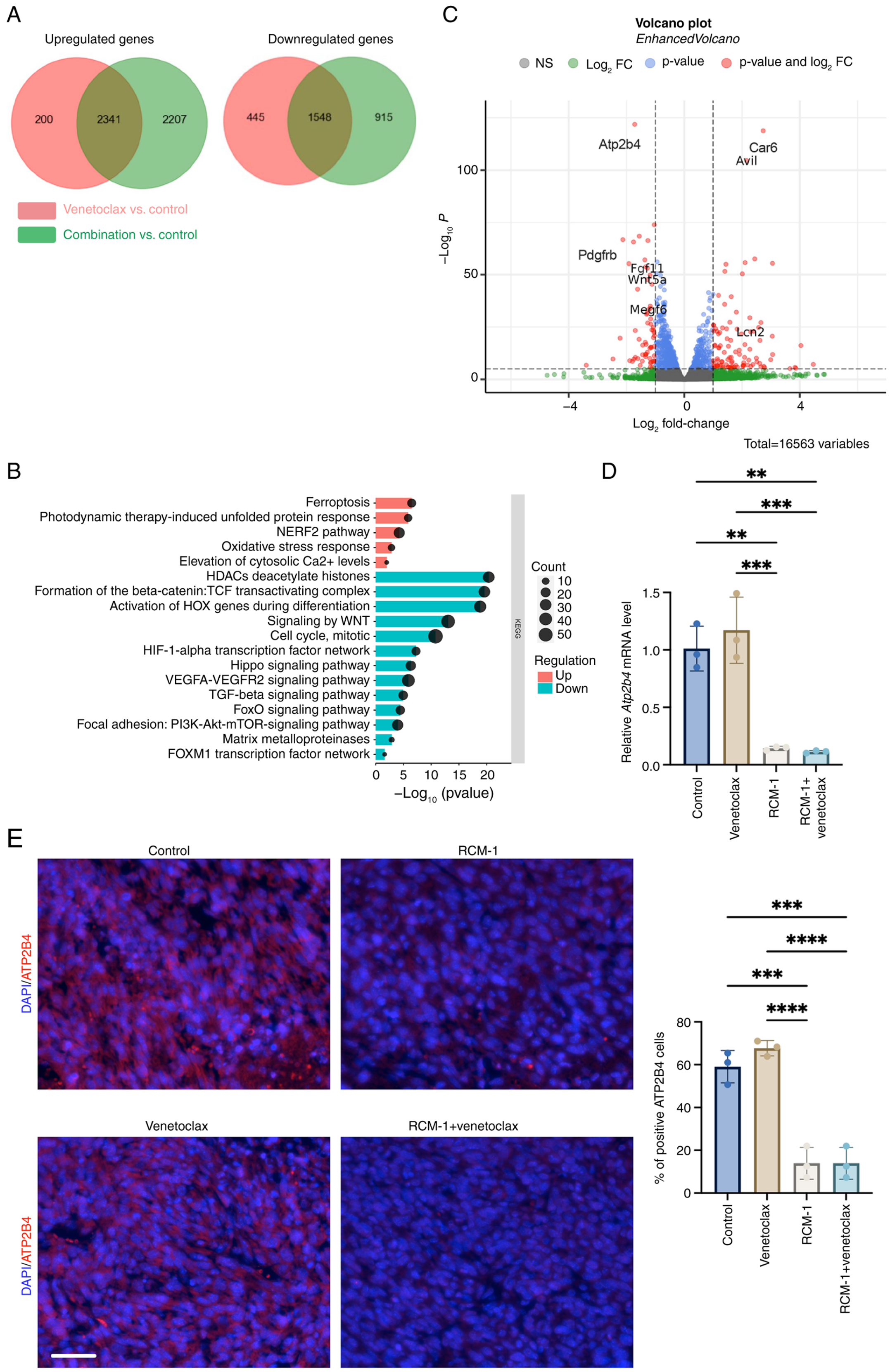

Figure 3. Combination treatment with RCM-1 and venetoclax reveals a unique genetic profile in 76-9 cells. (A) Venn diagrams illustrated the overlap of differentially expressed genes between the combination therapy and venetoclax compared with the control. (B) Gene set enrichment analysis of RNA-sequencing data highlighted the upregulated pathways in the combination therapy relative to venetoclax, such as ferroptosis and elevated cytosolic Ca^{+2} level, as well as the downregulated pathways, such as WNT signaling pathway, mitotic cell cycle and angiogenesis pathway. (C) Volcano plot identified the differentially expressed genes in the combination therapy vs. venetoclax. *Atp2b4* was notably downregulated in the combination therapy. (D) Reverse transcription-quantitative PCR showed the downregulation of *Atp2b4* in 76-9 cells treated with RCM-1 and combination therapy. *Actb* mRNA was used for normalization (E) Protein levels of ATP2B4 were decreased after RCM-1 and the combination treatments, as shown by immunofluorescence using ATP2B4 antibodies. A total of five random fields per sample were used to quantify the percentage of ATP2B4-positive cells per group. Scale bar, 10 μm. Data presented as mean ± SD. **P≤0.01, ***P≤0.001, ****P≤0.0001.

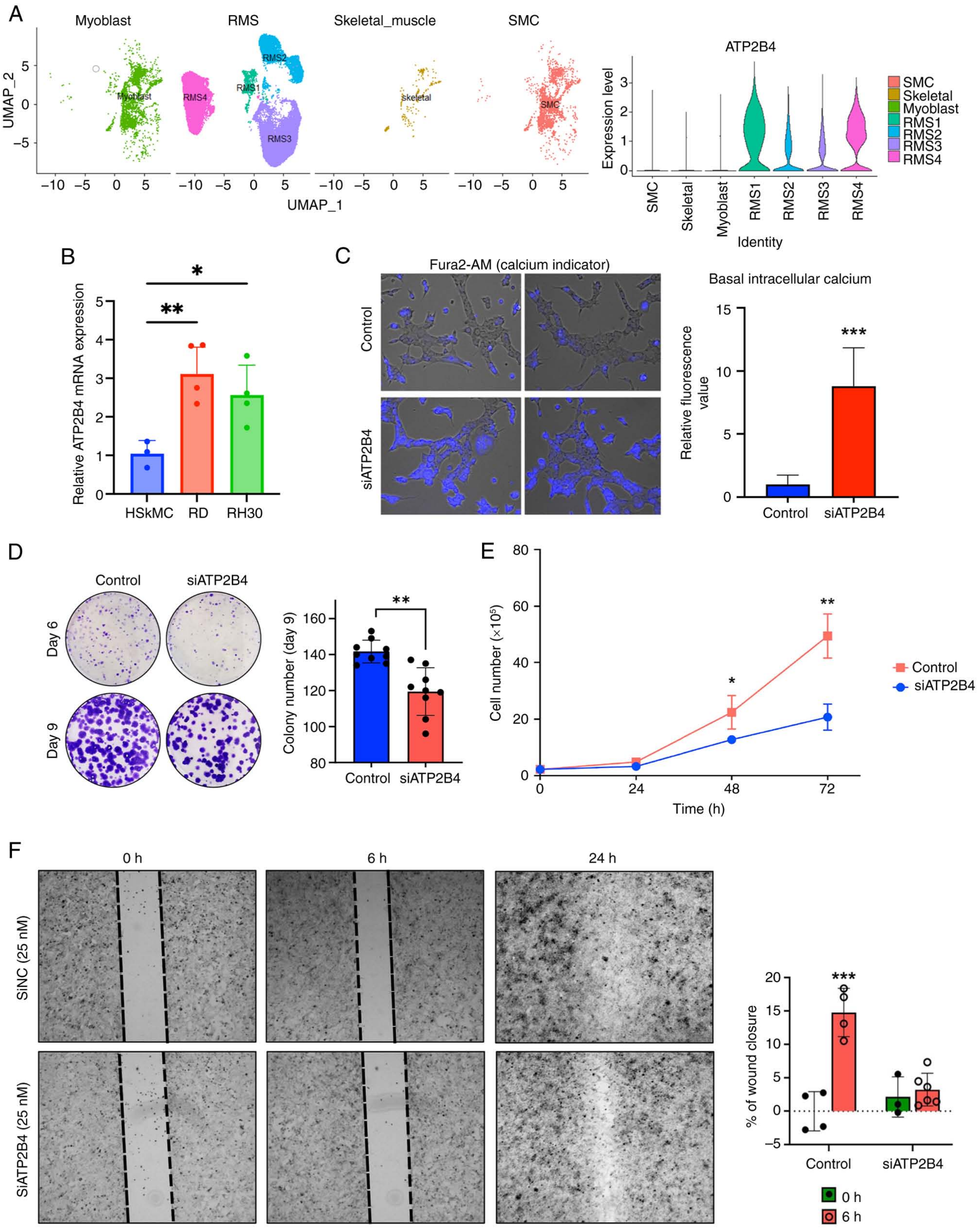

Figure 4. *ATP2B4* is differentially overexpressed in RMS cells vs. normal muscle cells and its knockdown decreases tumor cell proliferation, migration and colony formation. (A) Left panel, Human myoblast (muscle progenitor cells), RMS, normal skeletal muscle and smooth muscle scRNA sequencing datasets were visualized using UMAP. Data were extracted from GSE143704 for normal muscle tissue, GSE 195709 for RMS (RMS1 and 3 are fusion-negative RMS, RMS2 is fusion-positive and RMS4 is spindle (fusion-negative). Right panel, *ATP2B4* mRNA expression was higher in RMS cells compared with normal muscle cells. (B) Reverse transcription-quantitative PCR showed the upregulation of *ATP2B4* mRNA level in RMS cells (RD and RH30) compared with HSkMC. (C) Knockdown of *ATP2B4* increased the intracellular calcium level. Calcium level was assessed using the calcium-sensitive fluorescent dye fura-2 AM. Scale bar, 10 μm. (D) Knockdown of *ATP2B4* inhibited colony formation in 76-9 RMS cells. Data presented as mean ± SD. (E) Knockdown of *ATP2B4* suppressed 76-9 cell proliferation in culture. Data presented as mean ± SD. (F) *ATP2B4* knockdown decreased RMS cell migration. The percentage of wound closure presented as mean ± SD (magnification, x4). *P≤0.05, **P≤0.01, ***P≤0.001. RMS, rhabdomyosarcoma; UMAP, Uniform Manifold Approximation and Projection; HSkMC, human skeletal muscle cells; SMC, smooth muscle cells.

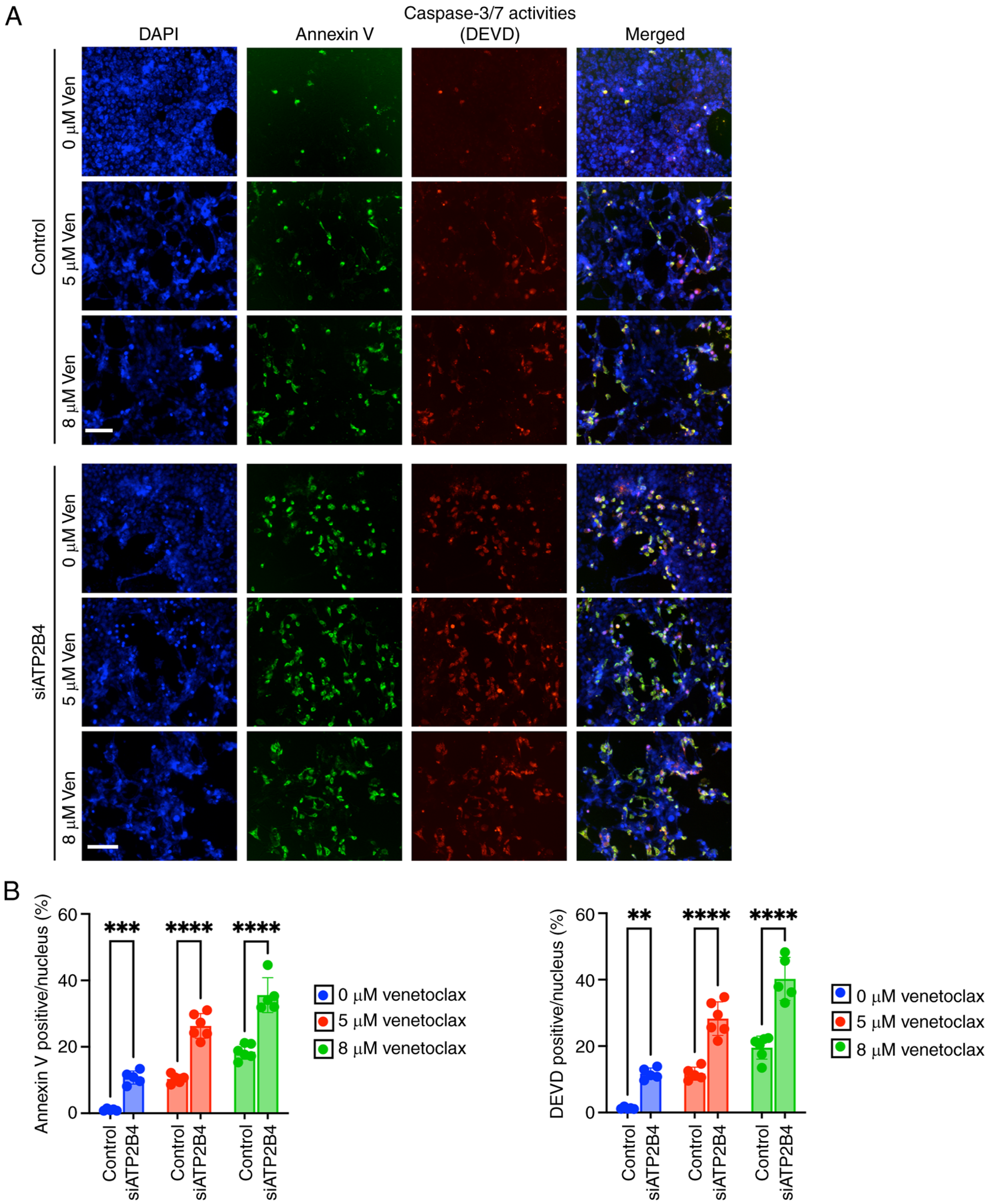

Figure 5. ATP2B4 knockdown enhances venetoclax-mediated apoptosis in 76-9 RMS cells. (A) Representative immunofluorescence images from control and siATP2B4 76-9 cells treated with DMSO, 5 and or 8 mM of venetoclax for 24 h. Venetoclax-induced dose-dependent apoptosis was measured by caspase 3/7 (DEVD) activity (red) and annexin V (green). Scale bar, 100 mm. The knockdown of *ATP2B4* increased RMS apoptosis compared with control cells. (B) The percentage of annexin and DEVD positive cells were counted in five random fields using the EVOS imaging software and presented as mean ± SD from triplicates of one experiment. $^{**}P\leq0.01$, $^{***}P\leq0.001$, $^{****}P\leq0.0001$. ATP2B4; ATPase Plasma Membrane Ca^{2+} Transporting 4; RMS, rhabdomyosarcoma.

of ATP2B4 in the siATP2B4-KD cells increased the efficacy of the same doses of venetoclax, which was demonstrated by a higher percentage of Annexin V-positive cells (10-35% in siATP2B4-KD vs. 1-18% in controls, P£0.0001) and DEVD-positive cells (10-40% vs. 1-20%, P<0.0001; Fig. 5A and B). Thus, depletion of ATP2B4 increases venetoclax-mediated apoptosis in 76-9 RMS cells.

ATP2B4 overexpression induces resistance to apoptosis and decreases the therapeutic effect of venetoclax in 76-9 RMS cells. As the depletion of ATP2B4 sensitized RMS cells to venetoclax-mediated apoptosis, the present study next determined whether overexpression of *Atp2b4* would inhibit venetoclax-mediated apoptosis. ATP2B4 has 2 main isoforms, 4a and 4b, with isoform 4b being more predominant and active in different

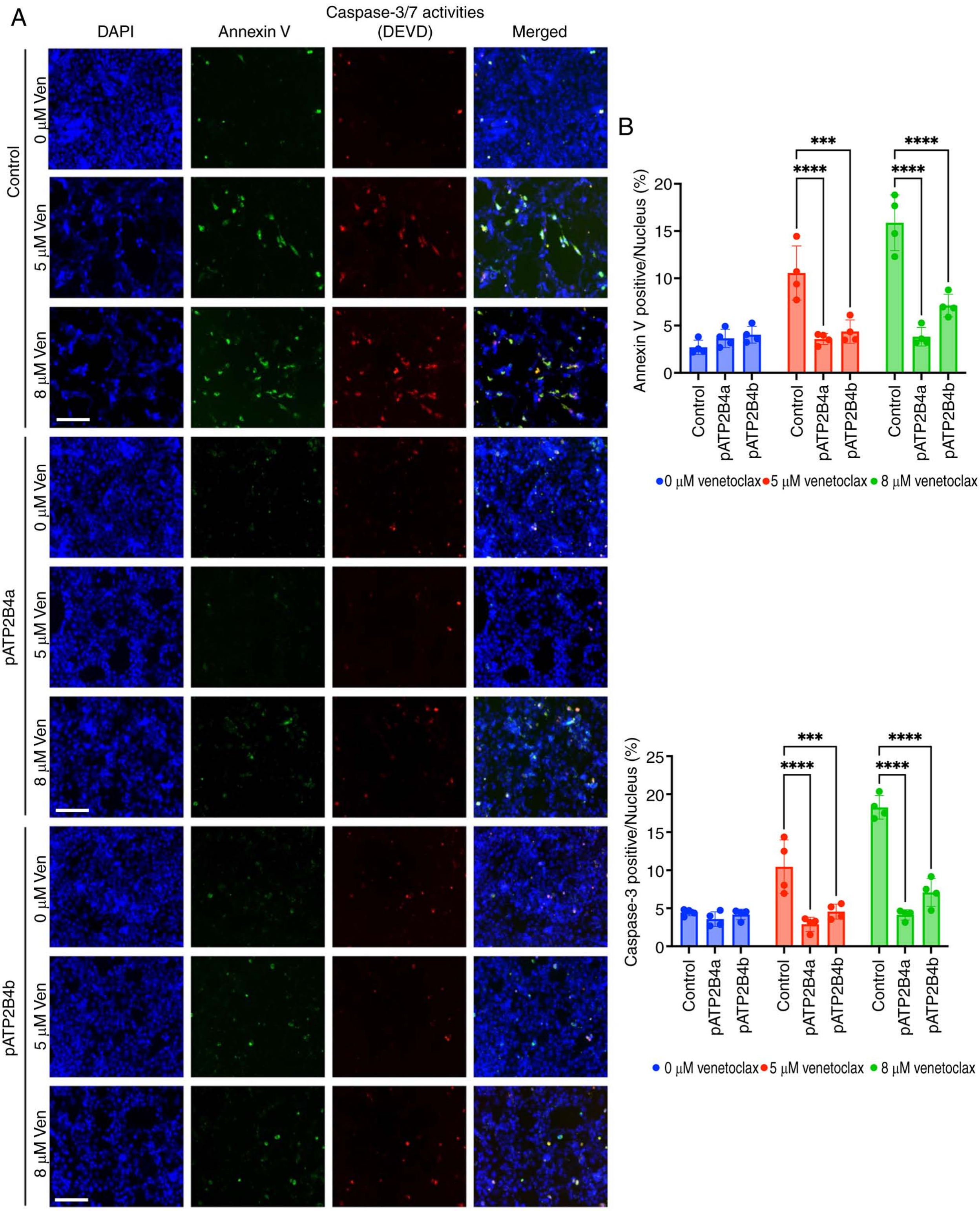

Figure 6. Overexpression of ATP2B4 increases the resistance of RMS cells to apoptosis. (A) Representative immunofluorescence images depicting control, pATP2B4a and pATP2B4b 76-9 cells treated with DMSO, 5 mM, or 8 mM of venetoclax for 24 h. The overexpression of both ATP2B4 isoforms reduced apoptosis compared with control RMS cells following venetoclax treatment. Scale bar, 100 mm. (B) The percentage of positive annexin and DEVD cells were counted in five random fields using the EVOS imaging software and presented as the mean ± SD from triplicates of one experiment. ***P≤0.001, ****P≤0.0001. ATP2B4; ATPase Plasma Membrane Ca^{2+} Transporting 4; RMS, rhabdomyosarcoma.

cancers (50). Therefore, the present study overexpressed *Atp2b4a* and *Atp2b4b* in 76-9 cells. The transfection efficiency was examined using RT-qPCR and immunofluorescence (Fig. S4B). The WT and pATP2B4 cells were treated with increasing doses of venetoclax. Overexpression of *Atp2b4* markedly decreased cellular apoptosis after venetoclax treatment, measured by decreased caspase 3/7 (DEVD) positive cells (3-8% in pATP2B4 vs. 4-18% in controls, P≤0.0001) and decreased cellular death, measured by decreased annexin positive cells (3-8% in pATP2B4 vs. 2-18% in controls, P≤0.0001; Fig. 6A and B). Thus, increasing

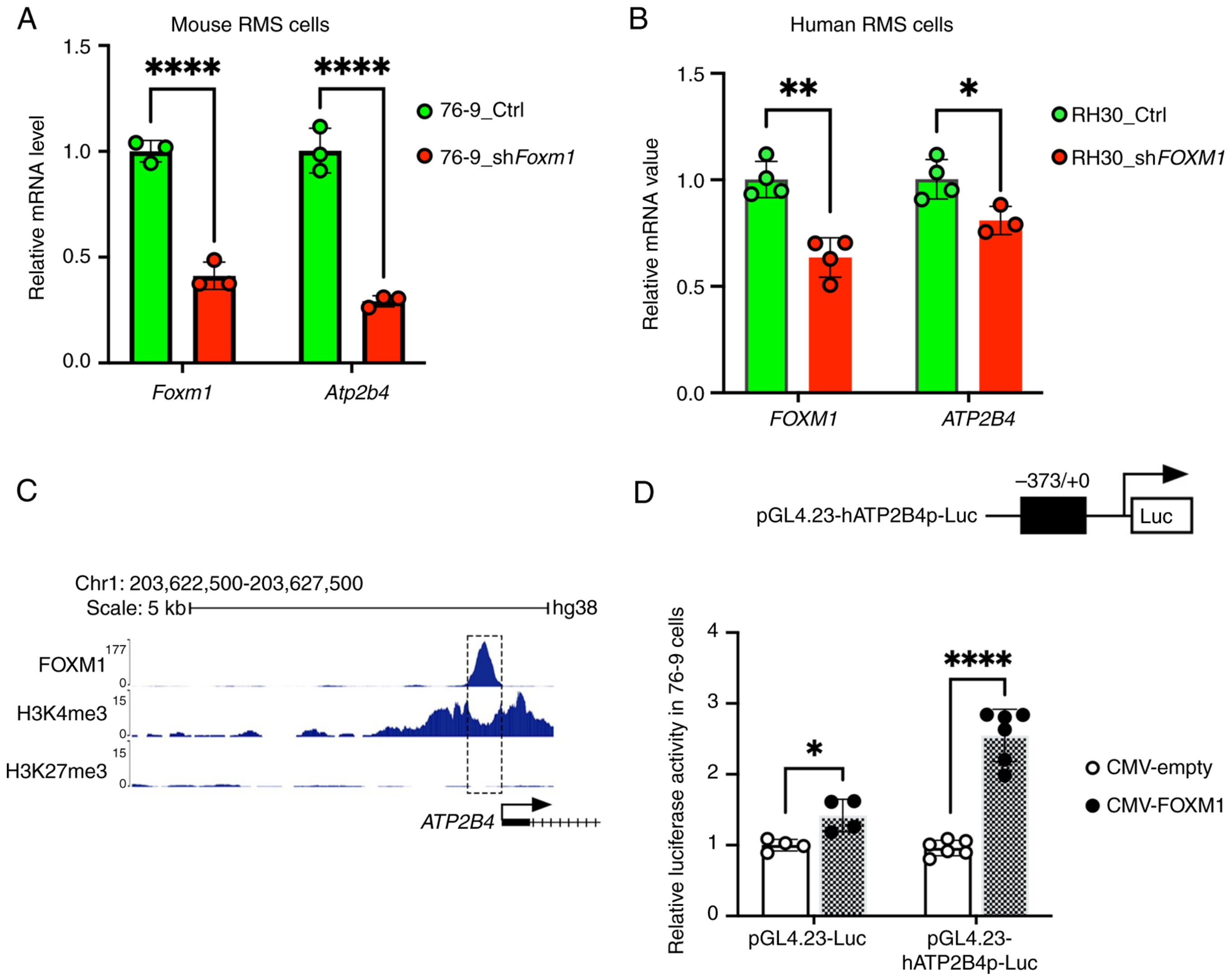

Figure 7. FOXM1 binds the ATP2B4 promotor and regulates the expression of ATP2B4 in RMS cells. (A) shRNA-mediated knockdown of *Foxm1* reduced *Atp2b4* mRNA in 76-9 murine RMS cells. RT-qPCR showed the efficient knockdown of *Foxm1* in 76-9 cells. n=3. P≤0.0001. (B) shRNA-mediated knockdown of *FOXM1* reduced *ATP2B4* mRNA in RH30 human RMS cells. RT-qPCR confirmed the efficient knockdown of *FOXM1* in RH30 cells. n=3. P≤0.01 (C) ChIP-seq showed the direct binding of FOXM1 protein to the *ATP2B4* promoter region in K562 (human lymphoblasts). (D) Upper panel, schematic drawing of the pGL4.23-ATP2B4-Luc construct. Lower panel, 76-9 cells were co-infected with the luciferase reporter, *Renilla* and either a CMV-empty or CMV-Foxm1 overexpressed plasmid. The CMV-Foxm1 expression vector increased the transcriptional activity of the *Atp2b4* promoter region compared with the CMV-empty vector (P<0.0001). *P≤0.05, **P≤0.01, ****P≤0.0001. FOXM1, Forkhead box protein M1; ATP2B4; ATPase Plasma Membrane Ca^{2+} Transporting 4; RMS, rhabdomyosarcoma; sh, short hairpin; RT-qPCR, reverse transcription-quantitative PCR.

ATP2B4 levels induces RMS resistance to apoptosis and decreases the therapeutic effect of venetoclax in RMS cells.

FOXM1 transcriptionally regulates ATP2B4 expression and RCM-1 downregulates ATP2B4 expression via FOXM1 inhibition. As it is known that RCM-1 specifically inhibits FOXM1 and we have shown that RCM-1 decreases ATP2B4 in RMS (Fig. 3D-E), the present study next examined whether FOXM1 directly regulated ATP2B4 in RMS. Mouse RMS cells were transfected with control and sh*Foxm1*. The shRNA-mediated knockdown of *Foxm1* in 76-9 decreased expression of *Atp2b4* mRNA (Fig. 7A). Similarly, shRNA-mediated knockdown of *FOXM1* in human RH30 rhabdomyosarcoma cells also decreased the expression of *ATP2B4* (Fig. 7B). Next, a publicly available ChIP-seq dataset from the ENCODE portal (51,52) was used and it was demonstrated that FOXM1 directly binds to the *ATP2B4* promoter region in cancer cells (Fig. 7C). The FOXM1-binding region in the *ATP2B4* promoter had H3K4me3 but not H3K27me3 marks, suggesting that FOXM1 activates the *ATP2B4* gene promoter (Fig. 7C). To verify that FOXM1 activates *ATP2B4* gene expression, the-373/+0 bp *ATP2B4* promoter region, containing the FOXM1-binding site identified by ChIP-seq (Fig. 7C), was cloned into the pGL4.23 luciferase reporter plasmid (Fig. 7D). In co-transfection experiments using mouse RMS cells, the CMV-Foxm1 expression vector increased transcriptional activity of the-373/+0 bp *ATP2B4* promoter region compared with CMV-empty vector (Fig. 7D). CMV-Foxm1 overexpression efficiency is shown in Fig. S5A. Thus, ATP2B4 is a direct transcriptional target of FOXM1 in rhabdomyosarcoma cells.

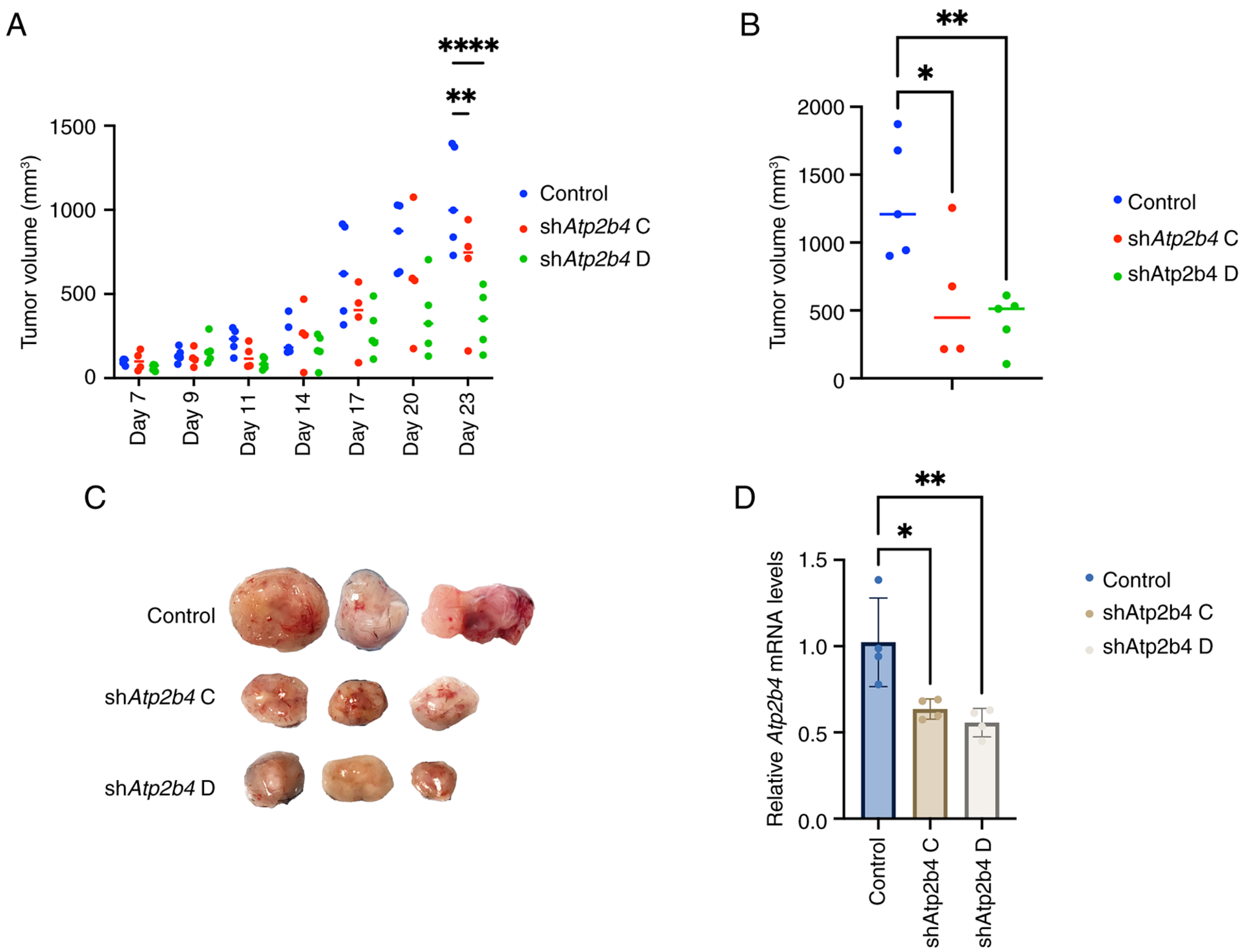

Figure 8. The knockdown of ATP2B4 slows RMS tumor growth. (A) Control and sh*Atp2b4* 76-9 cells were inoculated subcutaneously into the flank of C57Bl/6J mice. Tumor volume measured at different time points. Knockdown of ATP2B4 significantly impaired tumor growth compared with control mice (n=5 per group; presented as the mean ± SD). (B) Tumor volumes measured after tumor harvest show smaller sh*Atp2b4* tumors. The average vehicle tumor volume was 1,321 mm^3 compared with 592 mm^3 for *shAtp2b4* C and 468 mm^3 for *shAtp2b4* D. The maximum tumor diameter was 15.56x13.39 mm and the corresponding maximum tumor volume was 1,395 mm^3. (C) Gross images of control and sh*Atp2b4* RMS tumors. (D) Reverse transcription-quantitative PCR analysis of mRNA isolated from tumors confirmed ~50% knockdown efficiency in shAtp2b4-expressing tumors. *P≤0.05, **P≤0.01, ****P≤0.0001. ATP2B4; ATPase Plasma Membrane Ca^{2+} Transporting 4; RMS, rhabdomyosarcoma; sh, short hairpin.

Deletion of ATP2B4 inhibits RMS tumor growth in an animal model. As the depletion of ATP2B4 sensitized RMS cells to venetoclax-mediated apoptosis *in vitro*, the present study next determined the role of ATP2B4 knockdown in rhabdomyosarcoma growth in an animal model. 76-9 cells with stable deletion of *Atp2b4* were generated using sh*Atp2b4*. GFP-positive cells were isolated by FACS, followed by clonal expansion. Knockout efficiency was evaluated by RT-qPCR, revealing that sh*Atp2b4* C and sh*Atp2b4* D achieved the most substantial reduction in ATP2B4 expression, with knockdown levels of approximately 70-80%. (Fig. S6A). sh*Atp2b4* and control cells were then both subcutaneously injected into C57BL/6J mice. Deletion of *Atp2b4* decreased tumor growth and reduced final tumor volume compared with controls (Figs. 8A-C and S5B). RT-qPCR analysis of tumor-derived mRNA confirmed a knockdown efficiency of approximately 50% in the sh*Atp2b4* group (Fig. 8D). Immunostaining demonstrated that the protein level of ATP2B4 decreased in shAtp2b4 harboring tumors (Fig. S6B). Thus, efficient deletion of ATP2B4 inhibits RMS tumor growth in an animal model of RMS.

Discussion

Cytotoxic chemotherapy has been the cornerstone for the treatment of localized and metastatic rhabdomyosarcoma. Despite the heterogeneous genomic landscape of rhabdomyosarcoma, all types of childhood rhabdomyosarcomas are treated with similar cytotoxic agents (53). Multiple molecular targets have been identified as potential therapeutic hits in rhabdomyosarcoma, but the lack of efficacy or significant toxicity has halted the progress of these agents in clinical trials (54,55). Targeted therapies with less toxicity and better efficacy are an unmet need in rhabdomyosarcoma.

The present study evaluated a novel combination of RCM-1 and venetoclax in mouse and human rhabdomyosarcoma cell lines, as well as a mouse model of RMS. *FOXM1* is an oncogene that induces the transcription of many genes involved in cell cycle and DNA repair (56,57) However, the present study, to the best of the authors' knowledge, was the first to investigate the role of FOXM1 in regulating the expression of the ATP-dependent plasma membrane calcium channel, *ATP2B4*.

ATP2B is a family of calcium channels located on the plasma membrane and has a crucial role in extruding calcium and maintaining intracellular calcium hemostasis (58). ATP2B downregulation has been connected to intracellular calcium overload, cellular stress and death in different cancers (48,58). ATP2B is the predominant pathway in non-excitable cells and has 4 isoforms (ATP2B 1-4) (58). While ATP2B1 and ATP2B4 are ubiquitously expressed in tissues, ATP2B2 and ATP2B3 are predominantly expressed in excitable cells such as neurons (58). Knockdown of *ATP2B1* is lethal in embryos, indicating its crucial role in early embryo development. However, despite the extensive distribution in tissues, *ATP2B4* ablation is not lethal in embryos. This suggests that ATP2B4 may have specialized roles in disease pathogenesis and could serve as a potential therapeutic target in RMS.

FOXM1 binds the *ATP2B4* promoter and regulates its expression. RCM-1 via FOXM1 inhibition downregulates ATP2B4 expression and sensitizes RMS cells to venetoclax treatment. The present study showed that *ATP2B4* is overexpressed in rhabdomyosarcoma of different types compared with normal muscle and progenitor cells. Moreover, the present study showed that the knockdown of *ATP2B4* in rhabdomyosarcoma inhibits cell proliferation, colony formation and cell migration as well as tumor growth in a mouse model. Notably, the knockdown of *ATP2B4* enhanced the caspase-mediated apoptosis of venetoclax in rhabdomyosarcoma. On the other hand, *ATP2B4* overexpression resulted in increased resistance to apoptosis. The synergistic effect of RCM-1 and venetoclax may, in part, result from RCM-1-mediated downregulation of ATP2B4, although additional mechanisms are likely involved (19). The present study demonstrated that the decrease in ATP2B4 expression resulted in elevated intracellular calcium levels. Increased intracellular calcium has been linked to mitochondrial dysfunction, inhibiting Bcl2 and Bcl-XL while promoting BAK and BAX oligomerization, ultimately driving cells toward apoptosis (58). The enhanced apoptotic effect of venetoclax by the downregulation of ATP2B4 is also reported in breast cancer cells (48). Moreover, ATP2B4 overexpression confers worse survival outcomes in pancreatic adenocarcinoma and its inhibition sensitizes tumor cells to apoptosis (49,59). Notably, the role of ATP2B4 in cancer pathogenesis differs across types of cancer. For example, *ATP2B4* overexpression suppresses melanoma cell migration and induces colon and gastric cell differentiation (60-62). Nevertheless, these findings underscore the role of ATP2B4 in RMS pathobiology, highlighting its potential as a therapeutic target.

The present study was limited by the short observation period in the animal model, which may not fully capture long-term treatment effects. Additionally, patient-derived xenograft models of different types of RMS may give an improved reflection of tumor heterogeneity seen in patients compared with the murine xenografts used in the present study. Finally, future studies should evaluate the combination of RCM-1 and venetocalx across different types of rhabdomyosarcoma and in patient-derived xenograft models to facilitate its transition into early-phase clinical trials. Additional studies are warranted to identify biomarkers that may guide precision treatment and help identify patients who are most likely to benefit from this combination.

In conclusion, RCM-1 sensitizes rhabdomyosarcoma to venetoclax-induced apoptosis by inhibiting FOXM1 and downregulating *ATP2B4* expression. These findings highlight the potential therapeutic benefits of combining RCM-1 with venetoclax through the modulation of the calcium signaling pathway. This underscores the need for further investigation into this novel approach in rhabdomyosarcoma and supports exploring the calcium signaling pathway as a therapeutic strategy in rhabdomyosarcoma.

Acknowledgements

The call sets were downloaded from the ENCODE portal (63) (https://www.encodeproject.org/) with the following identifiers: ENCFF162QJJ, ENCFF660WUG and ENCFF139KZL.

Funding

The present study was supported by a CTI Research Grant, CancerFree KIDS to NM, Hyundai Hope on Wheels, Young Investigator Award to NM, NHLBI grant no. R01HL158659 to TVK and NHLBI grant no. R01HL141174 to VVK.

Availability of data and materials

The datasets generated during and/or analyzed during the current study are available in the NCBI Sequence Read Archive repository (SRA) under accession number: PRJNA1204196 (https://dataview.ncbi.nlm.nih.gov/object/PRJNA1204196?reviewer=mfdqbt192mum79u708ccn1r6od).

Authors' contributions

NM and TVK conceived and designed the study. NM and YWL performed the *in vivo* experiments. ZD designed and synthesized the nanoparticle. NM, YWL, XX, TJ and JDon participated *in vitro* and culture experiments. YWL and GW designed and performed the RNA-seq bioinformatics analysis. YWL and JDo designed and performed the dual luciferase analysis. NM and YWL analyzed data. NM, VVK and TVK interpreted the data. TVK and VVK provided critical reagents and intellectual discussions. NM and TVK wrote the paper. All authors discussed the data. NM and YWL confirmed the authenticity of all the raw data. TVK approved the submission of the manuscript. All authors read and approved the final manuscript.

Ethics approval and consent to participate

All animal studies were approved by the University of Arizona Institutional Animal Care and Use Committee and covered under animal protocol approval no. IACUC2023-1128).

Patient consent for publication

Not applicable.

Competing interests

The authors declare that they have no competing interests.

References

1. Martin-Giacalone BA, Weinstein PA, Plon SE and Lupo PJ: Pediatric rhabdomyosarcoma: Epidemiology and genetic susceptibility. J Clin Med 10: 2028, 2021.
2. McEvoy MT, Siegel DA, Dai S, Okcu MF, Zobeck M, Venkatramani R and Lupo PJ: Pediatric rhabdomyosarcoma incidence and survival in the United States: An assessment of 5656 cases, 2001-2017. Cancer Med 12: 3644-3656, 2023.
3. Oberlin O, Rey A, Lyden E, Bisogno G, Stevens MCG, Meyer WH, Carli M and Anderson JR: Prognostic factors in metastatic rhabdomyosarcomas: Results of a pooled analysis from United States and European cooperative groups. J Clin Oncol 26: 2384-2389, 2008.
4. Weigel BJ, Lyden E, Anderson JR, Meyer WH, Parham DM, Rodeberg DA, Michalski JM, Hawkins DS and Arndt CA: Intensive multiagent therapy, including dose-compressed cycles of ifosfamide/etoposide and vincristine/doxorubicin/cyclophosphamide, irinotecan, and radiation, in patients with high-risk rhabdomyosarcoma: A report from the children's oncology group. J Clin Oncol 34: 117-122, 2016.
5. Clark KL, Halay ED, Lai E and Burley SK: Co-crystal structure of the HNF-3/fork head DNA-recognition motif resembles histone H5. Nature 364: 412-420, 1993.
6. Kalin TV, Ustiyan V and Kalinichenko VV: Multiple faces of FoxM1 transcription factor: Lessons from transgenic mouse models. Cell Cycle 10: 396-405, 2011.
7. Milewski D, Balli D, Ustiyan V, Le T, Dienemann H, Warth A, Breuhahn K, Whitsett JA, Kalinichenko VV and Kalin TV: FOXM1 activates AGR2 and causes progression of lung adenomas into invasive mucinous adenocarcinomas. PLoS Genet 13: e1007097, 2017.
8. Weiler SME, Pinna F, Wolf T, Lutz T, Geldiyev A, Sticht C, Knaub M, Thomann S, Bissinger M, Wan S, *et al*: Induction of chromosome instability by activation of yes-associated protein and forkhead box M1 in liver cancer. Gastroenterology 152: 2037-2051.e22, 2017.
9. Cheng XH, Black M, Ustiyan V, Le T, Fulford L, Sridharan A, Medvedovic M, Kalinichenko VV, Whitsett JA and Kalin TV: SPDEF inhibits prostate carcinogenesis by disrupting a positive feedback loop in regulation of the Foxm1 oncogene. PLoS Genet 10: e1004656, 2014.
10. Wang IC, Ustiyan V, Zhang Y, Cai Y, Kalin TV and Kalinichenko VV: Foxm1 transcription factor is required for the initiation of lung tumorigenesis by oncogenic Kras(G12D.). Oncogene 33: 5391-5396, 2014.
11. Cai Y, Balli D, Ustiyan V, Fulford L, Hiller A, Misetic V, Zhang Y, Paluch AM, Waltz SE, Kasper S and Kalin TV: Foxm1 expression in prostate epithelial cells is essential for prostate carcinogenesis. J Biol Chem 288: 22527-22541, 2013.
12. Balli D, Ren X, Chou FS, Cross E, Zhang Y, Kalinichenko VV and Kalin TV: Foxm1 transcription factor is required for macrophage migration during lung inflammation and tumor formation. Oncogene 31: 3875-3888, 2012.
13. Li L, Wu D, Yu Q, Li L and Wu P: Prognostic value of FOXM1 in solid tumors: A systematic review and meta-analysis. Oncotarget 8: 32298-32308, 2017.
14. Kuda M, Kohashi K, Yamada Y, Maekawa A, Kinoshita Y, Nakatsura T, Iwamoto Y, Taguchi T and Oda Y: FOXM1 expression in rhabdomyosarcoma: A novel prognostic factor and therapeutic target. Tumour Biol 37: 5213-5223, 2016.
15. Nestal de Moraes G, Bella L, Zona S, Burton MJ and Lam EWF: Insights into a critical role of the FOXO3a-FOXM1 axis in DNA damage response and genotoxic drug resistance. Curr Drug Targets 17: 164-177, 2016.
16. Merjaneh N, Hajjar M, Lan YW, Kalinichenko VV and Kalin TV: The promise of combination therapies with FOXM1 inhibitors for cancer treatment. Cancers (Basel) 16: 756, 2024.
17. Ustiyan V, Zhang Y, Perl AKT, Whitsett JA, Kalin TV and Kalinichenko VV: β-catenin and Kras/Foxm1 signaling pathway are critical to restrict Sox9 in basal cells during pulmonary branching morphogenesis. Dev Dyn 245: 590-604, 2016.
18. Sun L, Ren X, Wang IC, Pradhan A, Zhang Y, Flood HM, Han B, Whitsett JA, Kalin TV and Kalinichenko VV: The FOXM1 inhibitor RCM-1 suppresses goblet cell metaplasia and prevents IL-13 and STAT6 signaling in allergen-exposed mice. Sci Signal 10: eaai8583, 2017.
19. Shukla S, Milewski D, Pradhan A, Rama N, Rice K, Le T, Flick MJ, Vaz S, Zhao X, Setchell KD, *et al*: The FOXM1 inhibitor RCM-1 decreases carcinogenesis and nuclear β-catenin. Mol Cancer Ther 18: 1217-1229, 2019.
20. Donovan J, Deng Z, Bian F, Shukla S, Gomez-Arroyo J, Shi D, Kalinichenko VV and Kalin TV: Improving anti-tumor efficacy of low-dose vincristine in rhabdomyosarcoma via the combination therapy with FOXM1 inhibitor RCM1. Front Oncol 13: 1112859, 2023.
21. Fairlie WD and Lee EF: Targeting the BCL-2-regulated apoptotic pathway for the treatment of solid cancers. Biochem Soc Trans 49: 2397-2410, 2021.
22. Steinert DM, Salganick J, Ballo M, Zhang W, Munsell M, Raney B, Jaffe N, Koh J, El-Naggar A and Trent J: Expression of Bax and Bcl-2 in human rhabdomyosarcoma: Correlation with survival in 64 patients. J Clin Oncol 23 (Suppl 16): S9041, 2005.
23. Armistead PM, Salganick J, Roh JS, Steinert DM, Patel S, Munsell M, El-Naggar AK, Benjamin RS, Zhang W and Trent JC: Expression of receptor tyrosine kinases and apoptotic molecules in rhabdomyosarcoma: Correlation with overall survival in 105 patients. Cancer 110: 2293-2303, 2007.
24. Ploumaki I, Triantafyllou E, Koumprentziotis IA, Karampinos K, Drougkas K, Karavolias I, Trontzas I and Kotteas EA: Bcl-2 pathway inhibition in solid tumors: A review of clinical trials. Clin Transl Oncol 25: 1554-1578, 2023.
25. Heinicke U, Haydn T, Kehr S, Vogler M and Fulda S: BCL-2 selective inhibitor ABT-199 primes rhabdomyosarcoma cells to histone deacetylase inhibitor-induced apoptosis. Oncogene 37: 5325-5339, 2018.
26. Alcon C, Manzano-Muñoz A, Prada E, Mora J, Soriano A, Guillén G, Gallego S, Roma J, Samitier J, Villanueva A and Montero J: Sequential combinations of chemotherapeutic agents with BH3 mimetics to treat rhabdomyosarcoma and avoid resistance. Cell Death Dis 11: 634, 2020.
27. Alcon C, Martín F, Prada E, Mora J, Soriano A, Guillén G, Gallego S, Roma J, Samitier J, Villanueva A and Montero J: MEK and MCL-1 sequential inhibition synergize to enhance rhabdomyosarcoma treatment. Cell Death Discov 8: 172, 2022.
28. Goldsmith KC, Verschuur A, Morgenstern DA, van Eijkelenburg N, Federico SM, Fraser C, Forlenza CJ, Ziegler DS, Gerber NU, Khaw AL, *et al*: The first report of pediatric patients with solid tumors treated with venetoclax. J Clin Oncol 38 (15 Suppl): S10524, 2020.
29. Hinson ARP, Jones R, Crose LES, Belyea BC, Barr FG and Linardic CM: Human rhabdomyosarcoma cell lines for rhabdomyosarcoma research: Utility and pitfalls. Front Oncol 3: 183, 2013.
30. Leddon JL, Chen CY, Currier MA, Wang PY, Jung FA, Denton NL, Cripe KM, Haworth KB, Arnold MA, Gross AC, *et al*: Oncolytic HSV virotherapy in murine sarcomas differentially triggers an antitumor T-cell response in the absence of virus permissivity. Mol Ther Oncolytics 1: 14010, 2015.
31. Milewski D, Pradhan A, Wang X, Cai Y, Le T, Turpin B, Kalinichenko VV and Kalin TV: FoxF1 and FoxF2 transcription factors synergistically promote rhabdomyosarcoma carcinogenesis by repressing transcription of $p21^{Cip1}$ CDK inhibitor. Oncogene 36: 850-862, 2017.
32. Sun F, Wang G, Pradhan A, Xu K, Gomez-Arroyo J, Zhang Y, Kalin GT, Deng Z, Vagnozzi RJ, He H, *et al*: Nanoparticle delivery of STAT3 alleviates pulmonary hypertension in a mouse model of alveolar capillary dysplasia. Circulation 144: 539-555, 2021.
33. Deng Z, Lin J, Bud'ko SL, Webster B, Kalin TV, Kalinichenko VV and Shi D: Dual targeting with cell surface electrical charge and folic acid via superparamagnetic Fe_3O_4@$Cu_{2-x}S$ for photothermal cancer cell killing. Cancers (Basel) 13: 5275, 2021.
34. Deng Z, Gao W, Kohram F, Li E, Kalin TV, Shi D and Kalinichenko VV: Fluorinated amphiphilic Poly(β-Amino ester) nanoparticle for highly efficient and specific delivery of nucleic acids to the Lung capillary endothelium. Bioact Mater 31: 1-17, 2023.
35. Milewski D, Shukla S, Gryder BE, Pradhan A, Donovan J, Sudha P, Vallabh S, Pyros A, Xu Y, Barski A, *et al*: FOXF1 is required for the oncogenic properties of PAX3-FOXO1 in rhabdomyosarcoma. Oncogene 40: 2182-2199, 2021.
36. Singh S, Uppuluri P, Mamouei Z, Alqarihi A, Elhassan H, French S, Lockhart SR, Chiller T, Edwards JE Jr and Ibrahim AS: The NDV-3A vaccine protects mice from multidrug resistant Candida auris infection. PLoS Pathog 15: e1007460, 2019.

37. Li Z, Wang H, Li S, Deng B, Zhang W, Wu P, Li W, Xin P, Zhao L and Gao S: Anti-pseudomonas aeruginosa activity of the scorpion-derived peptide GK8. Probiotics Antimicrob Proteins: Jul 3, 2025 (Epub ahead of print).
38. Acharya A, Bian F, Gomez-Arroyo J, Wagner KA, Kalinichenko VV and Kalin TV: Hypoxia represses FOXF1 in lung endothelial cells through HIF-1α. Front Physiol 14: 1309155, 2024.
39. Shukla S, Saha T, Rama N, Acharya A, Le T, Bian F, Donovan J, Tan LA, Vatner R, Kalinichenko V, *et al*: Ultra-high dose-rate proton FLASH improves tumor control. Radiother Oncol 186: 109741, 2023.
40. Livak KJ and Schmittgen TD: Analysis of relative gene expression data using real-time quantitative PCR and the 2(-Delta Delta C(T)) method. Methods 25: 402-408, 2001.
41. Love MI, Huber W and Anders S: Moderated estimation of fold change and dispersion for RNA-seq data with DESeq2. Genome Biol 15: 550, 2014.
42. Emig D, Salomonis N, Baumbach J, Lengauer T, Conklin BR and Albrecht M: AltAnalyze and DomainGraph: Analyzing and visualizing exon expression data. Nucleic Acids Res 38: W755-W762, 2010.
43. Chen J, Bardes EE, Aronow BJ and Jegga AG: ToppGene Suite for gene list enrichment analysis and candidate gene prioritization. Nucleic Acids Res 37: W305-W311, 2009.
44. Tang D, Chen M, Huang X, Zhang G, Zeng L, Zhang G, Wu S and Wang Y: SRplot: A free online platform for data visualization and graphing. PLoS One 18: e0294236, 2023.
45. De Micheli AJ, Spector JA, Elemento O and Cosgrove BD: A reference single-cell transcriptomic atlas of human skeletal muscle tissue reveals bifurcated muscle stem cell populations. Skelet Muscle 10: 19, 2020.
46. Wei Y, Qin Q, Yan C, Hayes MN, Garcia SP, Xi H, Do D, Jin AH, Eng TC, McCarthy KM, *et al*: Single-cell analysis and functional characterization uncover the stem cell hierarchies and developmental origins of rhabdomyosarcoma. Nat Cancer 3: 961-975, 2022.
47. Dalton KM, Krytska K, Lochmann TL, Sano R, Casey C, D'Aulerio A, Khan QA, Crowther GS, Coon C, Cai J, *et al*: Venetoclax-based rational combinations are effective in models of MYCN-amplified neuroblastoma. Mol Cancer Ther 20: 1400-1411, 2021.
48. Curry MC, Luk NA, Kenny PA, Roberts-Thomson SJ and Monteith GR: Distinct regulation of cytoplasmic calcium signals and cell death pathways by different plasma membrane calcium ATPase isoforms in MDA-MB-231 breast cancer cells. J Biol Chem 287: 28598-28608, 2012.
49. Sritangos P, Pena Alarcon E, James AD, Sultan A, Richardson DA and Bruce JIE: Plasma membrane Ca^{2+} ATPase isoform 4 (PMCA4) has an important role in numerous hallmarks of pancreatic cancer. Cancers (Basel) 12: 218, 2020.
50. Naffa R, Hegedűs L, Hegedűs T, Tóth S, Papp B, Tordai A and Enyedi Á: Plasma membrane Ca^{2+} pump isoform 4 function in cell migration and cancer metastasis. J Physiol 602: 1551-1564, 2024.
51. ENCODE Project Consortium: An integrated encyclopedia of DNA elements in the human genome. Nature 489: 57-74, 2012.
52. Zhang J, Liu J, Lee D, Lou S, Chen Z, Gürsoy G and Gerstein M: DiNeR: A differential graphical model for analysis of co-regulation network rewiring. BMC Bioinformatics 21: 281, 2020.
53. Ruymann FB: The development of VAC chemotherapy in rhabdomyosarcoma: What does one do for an encore? Curr Oncol Rep 5: 505-509, 2003.
54. Nguyen TH and Barr FG: Therapeutic approaches targeting PAX3-FOXO1 and its regulatory and transcriptional pathways in rhabdomyosarcoma. Molecules 23: 2798, 2018.
55. Chen C, Dorado Garcia H, Scheer M and Henssen AG: Current and future treatment strategies for rhabdomyosarcoma. Front Oncol 9: 1458, 2019.
56. Kalinichenko VV and Kalin TV: Is there potential to target FOXM1 for 'undruggable' lung cancers? Expert Opin Ther Targets 19: 865-867, 2015.
57. Black M, Arumugam P, Shukla S, Pradhan A, Ustiyan V, Milewski D, Kalinichenko VV and Kalin TV: FOXM1 nuclear transcription factor translocates into mitochondria and inhibits oxidative phosphorylation. Mol Biol Cell 31: 1411-1424, 2020.
58. Stafford N, Wilson C, Oceandy D, Neyses L and Cartwright EJ: The plasma membrane calcium ATPases and their role as major new players in human disease. Physiol Rev 97: 1089-1125, 2017.
59. James AD, Chan A, Erice O, Siriwardena AK and Bruce JIE: Glycolytic ATP fuels the plasma membrane calcium pump critical for pancreatic cancer cell survival. J Biol Chem 288: 36007-36019, 2013.
60. Hegedũs L, Garay T, Molnár E, Varga K, Bilecz Á, Török S, Padányi R, Pászty K, Wolf M, Grusch M, *et al*: The plasma membrane Ca^{2+} pump PMCA4b inhibits the migratory and metastatic activity of BRAF mutant melanoma cells. Int J Cancer 140: 2758-2770, 2017.
61. Ribiczey P, Tordai A, Andrikovics H, Filoteo AG, Penniston JT, Enouf J, Enyedi A, Papp B and Kovács T: Isoform-specific up-regulation of plasma membrane Ca2+ATPase expression during colon and gastric cancer cell differentiation. Cell Calcium 42: 590-605, 2007.
62. Aung C, Kruger W, Poronnik P, Roberts-Thomson S and Monteith G: Plasma membrane Ca2+-ATPase expression during colon cancer cell line differentiation. Biochem Biophys Res Commun 355: 932-936, 2007.
63. Sloan CA, Chan ET, Davidson JM, Malladi VS, Strattan JS, Hitz BC, Gabdank I, Narayanan AK, Ho M, Lee BT, *et al*: ENCODE data at the ENCODE portal. Nucleic Acids Res 44: D726-D732, 2016.